Search for Majorana Fermions in Multiband Semiconducting Nanowires

Roman M. Lutchyn,[1,3] Tudor D. Stanescu,[1,2] and S. Das Sarma[1]

[1]*Joint Quantum Institute and Condensed Matter Theory Center, Department of Physics, University of Maryland,
College Park, Maryland 20742-4111, USA*
[2]*Department of Physics, West Virginia University, Morgantown, West Virginia 26506, USA*
[3]*Microsoft Research, Station Q, Elings Hall, University of California, Santa Barbara, California 93106, USA*
(Received 3 August 2010; published 21 March 2011)

We study multiband semiconducting nanowires proximity-coupled with an *s*-wave superconductor. We show that, when an odd number of subbands are occupied, the system realizes a nontrivial topological state supporting Majorana modes. We study the topological quantum phase transition in this system and calculate the phase diagram as a function of the chemical potential and magnetic field. Our key finding is that multiband occupancy not only lifts the stringent constraint of one-dimensionality but also allows one to have higher carrier density in the nanowire, and as such multisubband nanowires are better suited for observing the Majorana particle. We study the robustness of the topological phase by including the effects of the short- and long-range disorder. We show that there is an optimal regime in the phase diagram ("sweet spot") where the topological state is to a large extent insensitive to the presence of disorder.

Looking for the elusive Majorana particles is one of the most active and exciting current topics in all of physics [1]. Although originally proposed as a model for neutrinos, the current search for Majorana particles is mostly taking place in condensed matter or atomic systems [2,3] where these mysterious particles, which are their own antiparticles, emerge as effective quasiparticles from an underlying fermionic Hamiltonian. Quite apart from the intrinsic interest associated with the exotic Majorana particles, the possibility that they can be used in carrying out fault-tolerant topological quantum computation [4] by suitably exploiting their non-Abelian braiding statistics gives an additional technological impetus in the subject. It has been known for a while [5–8] that, under suitable conditions, Majorana particles could exist at the ends of 1D nanowires in the presence of the appropriate superconducting (SC) pairing. Also, it has been recently shown that the network of Majorana wires can be used for braiding [9] and topological quantum computation [10]. Although the semiconducting (SM) nanowires [7,8] are promising candidates for observing the Majorana, experimental realization of these proposals is challenging because obtaining strictly 1D nanowires is a very demanding materials problem [11]. In this Letter, we establish that one dimensionality, i.e., the occupancy of one only subband in the nanowire, is completely unnecessary, and Majorana particles can exist under rather general and robust conditions even when several subbands are occupied in the nanowire. More importantly, we prove the remarkable counterintuitive result that the multisubband system is, in fact, better suited in observing the Majorana than the strict 1D limit. We carry out an analytic theory establishing our main results and provide support for it by independent numerical calculations. We also study the robustness of the topological phase against

short- and long-range disorder and show that there is an optimal parameter regime where the system is most stable with respect to disorder. We believe that our results would go a long way in providing the most suitable solid-state system for the eventual observation of the Majorana particles.

In this Letter, we propose to study Majorana physics in a SM quantum well based on, for example, InAs-AlSb heterostructure [12]. The active system consists of a SM with a strong spin-orbit interaction proximity-coupled with an *s*-wave SC; see Fig. 1(a). The rectangular quantum well has the dimensions L_z, L_y, and L_x as shown in Fig. 1(a). We consider here the case of a strong confinement in the $\hat{z}$ direction such that $L_z \ll L_y, L_x$ so that only the lowest subband with respect to the $\hat{z}$-axis eigenstates is occupied. Then, the single-particle Hamiltonian takes the usual form
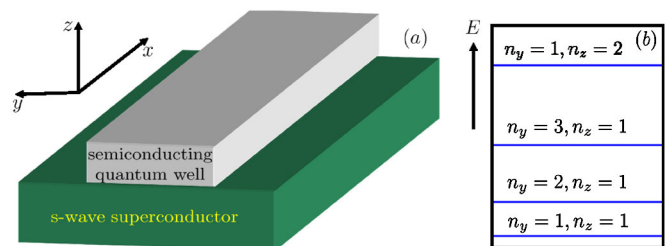

FIG. 1 (color online). (a) Schematic plot of the quasi-1D nanowire proximity-coupled with an *s*-wave SC. The rectangular quantum well has the dimensions L_z, L_y, and L_x: $L_z \ll L_y \ll L_x$. The nanowire can be top gated to control chemical potential in it. The method for fabricating the proposed quantum well heterostructure based on InAs has been demonstrated; see, e.g., Refs. [12,18].(b) Schematic plot of the lowest energy subbands due to the transverse confinement.

for the 2D SM in the presence of the spin-orbit Rashba interaction ($\hbar = 1$):

$$\mathcal{H}_{SM} = \int dx dy \, \psi_\sigma^\dagger(x, y) \hat{H}_{\sigma\sigma'} \psi_{\sigma'}(x, y), \qquad (1)$$

$$\hat{H} = -\frac{\partial_x^2 + \partial_y^2}{2m^*} - \mu - i\alpha(\sigma_x \partial_y - \sigma_y \partial_x) + V_x \sigma_x, \quad (2)$$

where m^*, α, and μ are the effective mass, the strength of spin-orbit interaction, and the chemical potential, respectively. The latter can be controlled by using the gate electrodes [11,12]. The last term in Eq. (2) corresponds to the Zeeman term due to the applied external magnetic field aligned along the $\hat{x}$ axis: $V_x = g_{SM}\mu_B B_x/2$. Note that the magnetic field is essential here—it opens up a gap in the spectrum at $p_x = 0$ and allows one to avoid fermion doubling, which is detrimental for the existence of Majorana fermions [7,8].

We now include the size quantization along the $\hat{y}$ direction by assuming that $L_y \ll L_x$. One can notice that Hamiltonian (2) is separable in x-y coordinates and the field operator can be written as

$$\psi(x, y) = \sum_{p_x, n_y = 1, 2, \dots} \sqrt{\frac{2}{L_y L_x}} \sin\left(\frac{\pi n_y y}{L_y}\right) e^{i p_x x} a_{p_x, n_y}, \quad (3)$$

where a_{p_x, n_y} is the electron annihilation operator in a state n_y having momentum p_x. The physical parameter regime we consider here corresponds to the confinement energy along the y direction being larger than all the relevant energy scales of the Hamiltonian (2) so that there are only a few lowest subbands occupied; see Fig. 1(b). This assumption actually corresponds to the typical experimental situation in InAs nanowires [13]. For $\mu < 2E_{sb}$, where $E_{sb} = 3\pi^2/2m^* L_y^2$ is the subband energy difference, one can project the wave function to the lowest two subbands $n_y = 1, 2$ in (3) and simplify the Hamiltonian (1). By introducing the spin-band spinors $\Phi = (c_{p_x\uparrow}, c_{p_x\downarrow}, d_{p_x\uparrow}, d_{p_x\downarrow})$, where the annihilation operators c_{p_x} and d_{p_x} correspond to $a_{p_x, n_y=1}$ and $a_{p_x, n_y=2}$, respectively, the single-body Hamiltonian becomes $\mathcal{H} = \sum_{p_x} \Phi^\dagger(p_x) H_{red} \Phi(p_x)$ with H_{red} being defined as

$$H_{red} = \frac{p_x^2}{2m^*} - \mu - \alpha\sigma_y p_x + E_{sb}\frac{1 - \rho_z}{2} - E_{bm}\sigma_x\rho_y + V_x\sigma_x.$$

Here Pauli matrices σ_i and ρ_i act on the spin and band degrees of freedom. The band mixing energy E_{bm} corresponds to the expectation value $\hat{p}_y$ operator between different band eigenstates, i.e., $E_{bm} = \int_0^{L_y} dy \frac{2\alpha}{L} \sin(\frac{2\pi y}{L}) \partial_y$ $\sin(\frac{\pi y}{L}) = \frac{8\alpha}{3L_y}$.

We now study topological properties in this regime with a low number of subbands occupied. We investigate here whether Majorana fermions survive and are robust in this

quasi-1D geometry. The multiband proximity-induced SC can be described as

$$H_{SC} = \sum_{p_x} [\Delta_{11} c_{p_x\uparrow}^\dagger c_{-p_x\downarrow}^\dagger + \Delta_{22} d_{p_x\uparrow}^\dagger d_{-p_x\downarrow}^\dagger + \Delta_{12} d_{p_x\uparrow}^\dagger c_{-p_x\downarrow}^\dagger$$
$$+ \Delta_{12} c_{p_x\uparrow}^\dagger d_{-p_x\downarrow}^\dagger + \text{H.c.}], \qquad (4)$$

where the induced SC pairing potentials Δ_{ij} depend on the microscopic details of the SM-SC interface, e.g., rough or smooth interface. In the former case the magnitude of Δ_{12} can be a sizable fraction of Δ_{11}. Taking into account the total Hamiltonian $H_{tot} = H_{red} + H_{SC}$ we can now define the Nambu spinor as follows: $\Psi(p) = (c_{p_x\uparrow}, c_{p_x\downarrow}, d_{p_x\uparrow}, d_{p_x\downarrow}, c_{-p_x\uparrow}^\dagger, c_{-p_x\downarrow}^\dagger, d_{-p_x\uparrow}^\dagger, d_{-p_x\downarrow}^\dagger)^T$. In this convention for Nambu spinors the Bogoliubov–de Gennes (BdG) Hamiltonian for two subband model reads

$$H_{BdG}(p_x) = \left(\frac{p_x^2}{2m^*} - \mu - \sigma_y p_x + \frac{E_{sb}}{2}(1 - \rho_z) + V_x\sigma_x\right)\tau_z$$
$$- E_{bm}\sigma_x\rho_y + i\sigma_y[\rho_x|\Delta_{12}| + \Delta_+ + \rho_z\Delta_-]$$
$$\times (i\tau_y \cos\varphi + i\tau_x \sin\varphi), \qquad (5)$$

where Pauli matrices σ_i, ρ_i, and τ_i act on spin, band, and Nambu degrees of freedom of the spinor $\Psi(p)$, respectively; $\Delta_\pm = (|\Delta_{11}| \pm |\Delta_{22}|)/2$, and φ is the SC phase. The particle-hole symmetry for H_{BdG} (5) reads $\Theta H_{BdG}(p)\Theta^{-1} = -H_{BdG}(-p)$, where Θ is an antiunitary operator $\Theta = \tau_x K$ with K denoting the complex conjugation.

The presence of Majorana modes in the system and the corresponding phase diagram can be obtained by using topological arguments due to Kitaev [5]. Following Ref. [5], we introduce Z_2 topological index $\mathcal{M}$ (Majorana number):

$$\mathcal{M} = \text{sgn}[\text{Pf}B(0)]\text{sgn}[\text{Pf}B(\pi/a)] = \pm 1, \qquad (6)$$

where ± 1 corresponds to topologically trivial and nontrivial states. Here antisymmetric matrix B defines the Hamiltonian of the system in the Majorana basis [5]. Rather than computing the transformation matrix to the Majorana basis as was originally done in Ref. [5], we note following Refs. [7,14] that the antisymmetric matrix $B(p_x)$ can be simply constructed by virtue of the particle-hole symmetry. Indeed, the matrix $B(P) = H_{BdG}(P)\tau_x$ needs to be calculated at the particle-hole invariant points where $H_{BdG}(P) = H_{BdG}(-P)$ and B is antisymmetric $B^T(P) = -B(P)$. In 1D there are two such points: $P = 0, \frac{\pi}{a}$ with $\frac{\pi}{a}$ being the momentum at the end of the Brillouin zone and a being the lattice spacing. (In the continuum limit $\pi/a \to \infty$.) The function Pf in Eq. (6) denotes Pfaffian of the antisymmetric matrix B. The computation of Pfaffian at $P = \pi/a \to \infty$ is straightforward yielding $\text{sgn}[\text{Pf}B(\pi/a)] = +1$. Thus, the phase boundary for the transition between topologically trivial and nontrivial phases is given by the sign change of $\text{Pf}B(0)$ which can

happen only when the bulk quasiparticle gap becomes zero, i.e., $\mathrm{Det}H_{\mathrm{BdG}}(P) = 0$; see Fig. 2. This is a generic phenomenon since the topological reconstruction of the fermionic spectrum cannot occur adiabatically and requires the nullification of the bulk excitation gap [15,16]. For a two-band model Pf$B(0)$ can be calculated analytically:

$$\begin{aligned}
\mathrm{Pf}B(0) = &\,(V_x^2 - E_{\mathrm{bm}}^2 + |\Delta_{12}|^2 + \Delta_-^2 - \Delta_+^2 - E_{\mathrm{sb}}\mu + \mu^2)^2 \\
&- V_x^2[E_{\mathrm{sb}}^2 - 4E_{\mathrm{sb}}\mu + 4(\Delta_{12}^2 + \Delta_-^2 + \mu^2)] \\
&+ [E_{\mathrm{sb}}(\Delta_- + \Delta_+) - 2\Delta_+\mu]^2,
\end{aligned} \tag{7}$$

allowing one to compute $\mathcal{M}$ as a function of the physical parameters. The phase diagram showing a sequence of topological phase transitions for the two subband nanowire is shown in Fig. 2(a). We now analyze the phase diagram in various regimes. In the limit $\mu, |V_x| \ll E_{\mathrm{sb}}$ we find that $\mathrm{Pf}B(0) \approx -V_x^2 + \Delta_{11}^2 + \mu^2$ recovering the previous results obtained for the single band [7,8]. When $|V_x| \ll \mu \sim E_{\mathrm{sb}}$ we find that $\mathrm{Pf}B(0) \approx -V_x^2 + \Delta_{22}^2 + (E_{\mathrm{sb}} - \mu)^2$. Thus, the system supports Majorana modes as long as $|V_x| > \sqrt{\Delta_{22}^2 + (E_{\mathrm{sb}} - \mu)^2}$. These results can be intuitively understood within the weak-coupling approximation
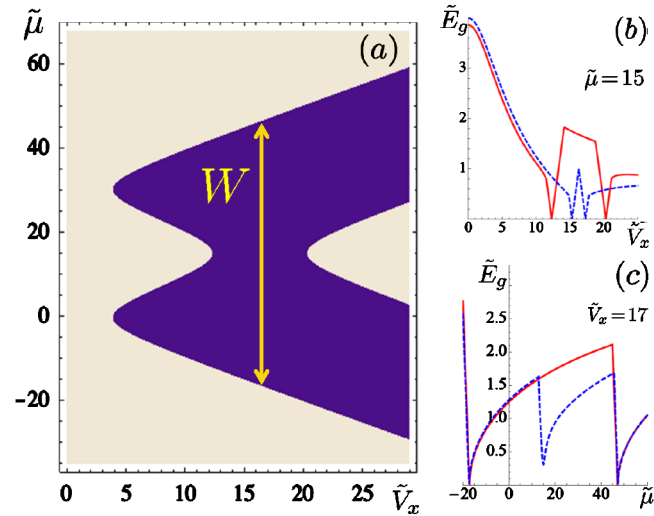

FIG. 2 (color online).   (a) Phase diagram for the two-band nanowire model as a function of the chemical potential $\tilde{\mu}$ and external magnetic field $\tilde{V}_x$. The width of the topological region is largest at the sweet spot: $\tilde{W} \approx 60$. Here the tilde denotes rescaled energy $\tilde{E} = E/m^*\alpha^2$ and $\tilde{\Delta}_{12} = 4$. The light and dark regions correspond to topologically trivial and nontrivial phases. (b), (c) Quasiparticle excitation gap obtained by using Eq. (5) as a function of $\tilde{V}_x$ and $\tilde{\mu}$. The solid (red) and dashed (blue) lines correspond to $\tilde{\Delta}_{12} = 4$ and $\tilde{\Delta}_{12} = 1$, respectively. The closing of the gap for $\tilde{\Delta}_{12} = 4$ (solid red line) is consistent with the phase diagram shown in (a). The quasiparticle excitation gap at the sweet spot strongly depends on the magnitude of $\tilde{\Delta}_{12}$. We assume here $m^* = 0.04m_e$ with m_e being electron mass and $\alpha = 0.1$ eV Å yielding $m^*\alpha^2 \approx 0.6$ K. We used realistic parameters $L_y = 130$ nm and $\tilde{E}_{\mathrm{sb}} = 30$, $\tilde{E}_{\mathrm{bm}} = 5$, and $\tilde{\Delta}_{11} = \tilde{\Delta}_{22} = 4$.

since in both cases the Fermi level crosses an odd number of bands in the interval $(0, \frac{\pi}{a})$. The most interesting parameter regime is $\mu \sim E_{\mathrm{sb}}/2$, which corresponds to the "sweet spot" in the phase diagram; see Fig. 2(a). At this point the system is to a large extent insensitive to chemical potential fluctuations, and, thus, this regime provides a promising route to realizing a robust topological SC phase. At $\mu = E_{\mathrm{sb}}/2$ the width of the topologically nontrivial region is given by $E_{\mathrm{sb}}/2 - \Delta_{12} < |V_x| < E_{\mathrm{sb}}/2 + \Delta_{12}$ to a leading order in $1/E_{\mathrm{sb}}$. This is a nonperturbative result, and the SC state emerging here is determined by the strong interband mixing due to Δ_{12}. The presence of a sizable Δ_{12} is crucial for the topological stability of the nontrivial SC phase, and the magnitude of the quasiparticle excitation gap at the sweet spot strongly depends on the value of Δ_{12}; see Figs. 2(b) and 2(c).

In order to establish the robustness of the topological phase near the sweet spot, we have done numerical simulations for a finite multiband nanowire with $L_x \sim 10 \ \mu$m and $L_y \sim 0.1 \ \mu$m. The results obtained by numerical diagonalization of the real-space Hamiltonian $H_{\mathrm{tot}} = H_{\mathrm{SM}} + H_{\mathrm{SC}}$ are shown in Figs. 3(a) and 3(b). One can notice that at the sweet spot ($\tilde{V}_x \approx 15$ and $\tilde{\mu} \approx 15$) there is a pair of Majorana zero-energy states whereas for a smaller magnetic field ($\tilde{V}_x \approx 8$) corresponding to the trivial phase the zero-energy modes disappear, corroborating the phase diagram shown in Fig. 2(a). Furthermore, at the sweet spot the zero-energy states are well-separated from the continuum. Indeed, as shown in Fig. 3(a), the minigap E_{mn} constitutes a sizable fraction of the induced SC gap: $E_{\mathrm{mn}} \sim 1$ K. Thus, Majorana modes in quasi-1D nanowires are very robust against thermal fluctuations which makes these systems very advantageous for the topological quantum computation. We also studied the robustness of the topological phase against disorder by adding the impurity potential $U_{\mathrm{imp}}(\mathbf{r}) = \sum_j U_{0j} \frac{\exp(-|\mathbf{r}-\mathbf{r}_j|/\lambda)}{1+|\mathbf{r}-\mathbf{r}_j|/d}$ to the Hamiltonian H_{tot}. Here $\mathbf{r}$ is a vector in the x-y plane, $\mathbf{r}_j$ are random positions of the impurities, λ is the screening length, $U_{0j} = \pm U_0$ is the impurity potential with a random sign but a constant magnitude U_0, and d is the cutoff regularizing $1/r$ potential at short distances. We considered here two types of disorder mimicking short-range impurities ($\lambda = 16$ nm) and long-range chemical potential fluctuations ($\lambda = 260$ nm); see Figs. 3(c) and 3(d). In the former case, the topological phase is very robust against disorder even if $|U_0| \gg E_{\mathrm{sb}}$; see Fig. 3(c). This can be qualitatively understood as follows: At a given position, the disorder potential leads to a formation of two Majorana modes localized at the impurity. Because these Majorana states are close to each other, they hybridize and form conventional subgap states and do not affect Majorana modes at the ends even if the impurity is fairly close to the edge; see Fig. 3(c). On the other hand, the long-range disorder is more dangerous. In Fig. 3(d), we show the energy spectrum for two cases: U_0 smaller ($\tilde{U}_0 = 25$) and larger ($\tilde{U}_0 = 100$) than $W/2$;
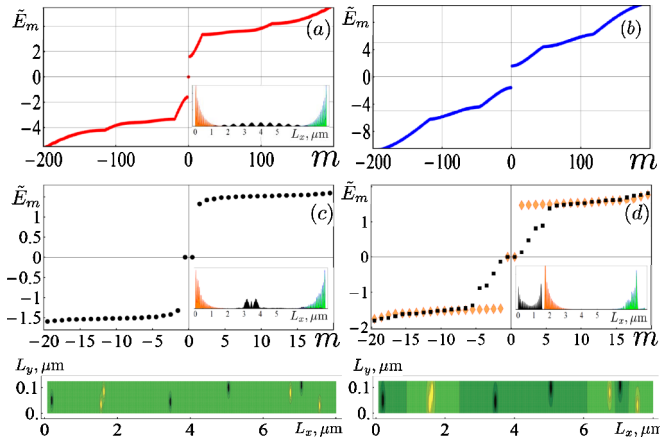
FIG. 3 (color online). (a),(b) Energy spectrum $\tilde{E}_m$ for a finite-size nanowire obtained by numerical diagonalization of $H_{\text{tot}} = H_{\text{SM}} + H_{\text{SC}}$ for $\tilde{\mu} = 15$, $\tilde{V}_x = 15$, and $\tilde{V}_x \approx 8$, respectively. Here $\tilde{E} = E/m^*\alpha^2$, and m labels eigenvalues of H_{tot}. Inset: Lowest-lying energy states. Majorana zero-energy modes are present in (a) and disappear in (b). (c),(d) Energy spectra for a given disorder realization with impurity potentials shown at the bottom of (c) and (d) corresponding to $\lambda = 16$ nm and $\lambda = 260$ nm, respectively. The dark (light) colors denote positive (negative) U_{0j}. (c) The spectrum at the sweet spot for the short-range disorder shown at the bottom ($\tilde{U}_0 = 100$). Inset: Lowest-lying eigenstates. The topological phase is robust against short-range disorder; i.e., the disorder affects extended states but leaves Majorana modes intact. (d) The spectrum at the sweet spot with long-range disorder for $\tilde{U}_0 = 100$ (squares) and $\tilde{U}_0 = 25$ (diamonds). The impurity potential U_{imp} is shown at the bottom of the panel. Inset: Lowest-lying eigenstates for $\tilde{U}_0 = 100$. The topological phase is stable as long as $U_0 < W/2$. For $\tilde{U}_0 = 100$ additional Majorana modes are localized at the impurities, and the topological phase collapses by splitting into fragments of topological and nontopological regions; see the inset. Both types of disorder lead to the emergence of the additional subgap states localized at the ends. Here we used parameters specified in Fig. 2.

see Fig. 2(a). For $U_0 < W/2$, the topological phase is stable; i.e., the disorder can suppress excitation gap but does not affect Majorana modes. On the other hand, if $U_0 > W/2$, the disorder effectively creates an inhomogeneous wire with many topological and nontopological regions [see Fig. 3(d)]. Thus, our simulations explicitly demonstrate the importance of working at the sweet spot where the width of the topological region W is maximized and the topological phase is most robust against long-range disorder.

In conclusion, we have derived the topological phase diagram for the existence of Majorana particles in a realistic quasi-1D semiconductor wire in the presence of multisubband occupancy. Unexpectedly, we find robust and experimentally feasible sweet spots in the chemical potential-Zeeman splitting phase diagram where Majorana modes should stabilize at the ends of the wire. The

great advantages of our proposed structure in detecting Majorana particles are (i) its materials flexibility (i.e., no need to impose one dimensionality or single channel constraint) and (ii) its immunity to density (or chemical potential) fluctuations and disorder. The calculation of the energy spectrum for realistic experimental settings suggests the possibility to test our theoretical results by using local tunneling experiments; see Ref. [17]. Tunneling of electrons to the ends of the nanowire would reveal a pronounced zero-bias peak when the system is in the topologically nontrivial phase. This zero-bias peak will disappear in the trivial phase.

Note added.—While finishing this manuscript we became aware of Refs. [3,19], where multichannel generalization of the spinless p-wave SC state was studied.

[1] F. Wilczek, Nature Phys. **5**, 614 (2009); M. Franz, Physics **3**, 24 (2010); A. Stern, Nature (London) **464**, 187 (2010).
[2] S. Das Sarma, M. Freedman, and C. Nayak, Phys. Rev. Lett. **94**, 166802 (2005); S. Tewari *et al.*, Phys. Rev. Lett. **98**, 010506 (2007); L. Fu and C. L. Kane, Phys. Rev. Lett. **100**, 096407 (2008); C. Zhang *et al.*, Phys. Rev. Lett. **101**, 160401 (2008); M. Sato, Y. Takahashi, and S. Fujimoto, Phys. Rev. Lett. **103**, 020401 (2009); G. E. Volovik, JETP Lett. **90**, 398 (2009); J. D. Sau *et al.*, Phys. Rev. Lett. **104**, 040502 (2010); J. Alicea, Phys. Rev. B **81**, 125318 (2010); J. Linder *et al.*, Phys. Rev. Lett. **104**, 067001 (2010).
[3] M. Wimmer *et al.*, Phys. Rev. Lett. **105**, 046803 (2010).
[4] C. Nayak *et al.*, Rev. Mod. Phys. **80**, 1083 (2008).
[5] A. Y. Kitaev, Phys. Usp. **44**, 131 (2001).
[6] L. Fu and C. L. Kane, Phys. Rev. B **79**, 161408(R) (2009).
[7] R. M. Lutchyn, J. D. Sau, and S. Das Sarma, Phys. Rev. Lett. **105**, 077001 (2010).
[8] Y. Oreg, G. Refael, and F. von Oppen, Phys. Rev. Lett. **105**, 177002 (2010).
[9] J. Alicea *et al.*, Nature Phys. (in press).
[10] F. Hassler *et al.*, New J. Phys. **12**, 125002 (2010); J. D. Sau, S. Tewari, and S. Das Sarma, Phys. Rev. A **82**, 052322 (2010).
[11] Y.-J. Doh *et al.*, Science **309**, 272 (2005); J. A. Van Dam *et al.*, Nature (London) **442**, 667 (2006).
[12] M. Thomas *et al.*, Phys. Rev. B **58**, 11 676 (1998).
[13] L. P. Kouwenhoven (private communication).
[14] P. Ghosh *et al.*, Phys. Rev. B **82**, 184525 (2010).
[15] N. Read and D. Green, Phys. Rev. B **61**, 10267 (2000).
[16] M. A. Silaev and G. E. Volovik, J. Low Temp. Phys. **161**, 460 (2010).
[17] K. T. Law, P. A. Lee, and T. K. Ng, Phys. Rev. Lett. **103**, 237001 (2009); J. D. Sau *et al.*, Phys. Rev. B **82**, 214509 (2010).
[18] H. Takayanagi and T. Kawakami, Phys. Rev. Lett. **54**, 2449 (1985).
[19] A. C. Potter and P. A. Lee, Phys. Rev. Lett. **105**, 227003 (2010).